Decomposition-Based Assembly Synthesis for Structural Stiffness

Naesung Lyu

Kazuhiro Saitou
e-mail: {nlyu,kazu}@umich.edu

Department of Mechanical Engineering,
University of Michigan, Ann Arbor, MI

This paper presents a method that systematically decomposes product geometry into a set of components considering the structural stiffness of the end product. A structure is represented as a graph of its topology, and the optimal decomposition is obtained by combining FEM analyses with a Genetic Algorithm. As the first case study, the side frame of a passenger car is decomposed for the minimum distortion of the front door panel geometry. As the second case study, the under body frame of a passenger car is decomposed for the minimum frame distortion. In both case studies, spot-weld joints are considered as joining methods, where each joint, which may contain multiple weld spots, is modeled as a torsional spring. First, the rates of the torsional springs are treated as constant values obtained in the literature. Second, they are treated as design variables within realistic bounds. By allowing the change in the joint rates, it is demonstrated that the optimal decomposition can achieve the smaller distortion with less amount of joint stiffness (hence less welding spots), than the optimal decomposition with the typical joint rates available in the literature. [DOI: 10.1115/1.1582879]

1 Introduction

To design any structural product, engineers adopt one of the two design methods: top-down and bottom-up methods. As the end products become more complicated and highly integrated, the top-down method is preferred since it allows the easier design assessment of an entire product during the design process. Top-down methods typically start with the preliminary design of the overall end product structure and proceed with the detailed design of components and substructures. If geometries and desired functions are simple, the structure can be built in one piece. To build complex structures in one piece, however, engineers need sophisticated manufacturing methods that would likely result in the higher manufacturing cost. Also, one piece structure will suffer from the lack of modularity: it would require the change or replacement of the entire structure even for local design changes or failures. It would be often natural, therefore, to design a structural product as an assembly of components with simpler geometries.

To design multi-component structural products in top-down fashion, an overall product geometry must be decomposed at some point during the design process. In industry, such decompositions are typically done prior to the detailed design of individual components, taking into account of geometry, functionality, and manufacturability issues. However, this process is usually non-systematic and hence might result in a decomposition overlooking the integrity of the end product. For instance, automotive industry utilizes a handful of basic decomposition schemes of a vehicle that have not been changed for decades. This is because the desired form, functionality, materials, joining methods, and weight distribution of mass-production vehicles have not changed much for decades. However, the conventional decomposition schemes may no longer be valid for the vehicles with new technologies such as space frame, lightweight materials, and fuel cell or battery powered motors, which would have dramatically different structural properties, weight distribution, and packaging requirements. This motivates the development of a systematic decomposition methodology presented in this paper.

In our previous work [1–3], we have termed assembly synthesis as the decision of which component set can achieve a desired function of the end product when assembled together, and assembly synthesis is achieved by the decomposition of product geom-etry. Since assembly process generally accounts for more than 50% of manufacturing costs and also affects the product quality [4], assembly synthesis would have a large impact on the quality and cost of the end product.

As an extension of our previous work, this paper introduces a method for decomposing a product geometry considering the *structural stiffness* of the end product. Because decomposition will determine the location of the joints between components, the structural integrity (e.g., stiffness) of the end-product will be heavily influenced by the choice of a particular decomposition. Designers can use this method to get feedback on the possible decompositions before the detailed design stage. Via the decomposition of a graph representing its topology, a product is decomposed into a candidate set of components with simpler geometries, where joints among components are modeled as torsional springs. By combining FEM analyses with Genetic Algorithms [5,6], the optimal decomposition that gives the desired structural property of the end product is obtained. The case studies discuss the assembly synthesis of the side door panels (Case Study 1) and under body frame of a passenger car (Case Study 2).

2 Related Work

2.1 Design for Assembly and Assembly Sequence Design. Many attempts have been made on assembly design and planning for decades. Among them, Boothroyd and Dewhurst [7] are widely regarded as major contributors in the formalization of design for assembly (DFA) concept. In their method [8], assembly costs are first reduced by the reduction of part count, followed by the local design changes of the remaining parts to enhance their assembleability and manufacturability. This basic approach is adopted by most subsequent works on DFA. There are a number of researchers investigating the integration of DFA and assembly sequence planning [9,10], where assembly sequence planning is proposed as the enumeration of geometrically feasible cut-sets of a liaison graph, an undirected graph representing the connectivity among components in an assembly. The local design changes are made to the components to improve the quality of the best assembly sequence. These works, however, focus on the local design changes of a given assembly design (i.e., already ''decomposed'' product design), and have less emphasis on how to synthesize an assembly to start with.

2.2 Automotive Body Structure Modeling. In automotive body structure, high stiffness is one of the most important design
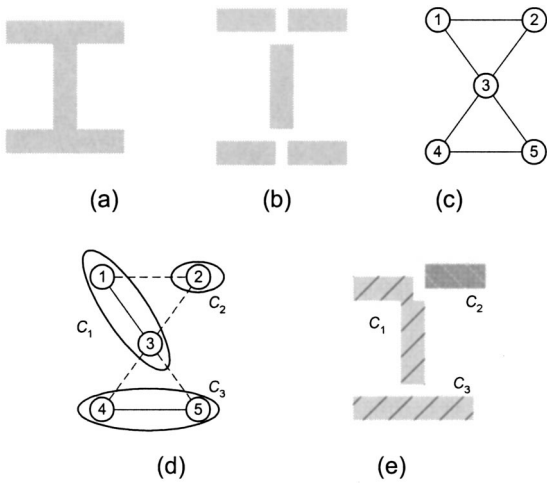
Fig. 1 Outline of the decomposition procedure. (a) structure to be decomposed, (b) basic members and potential joint locations, (c) structural topology graph G, (d) optimal decomposition of G, and (e) resulting decomposition of the original structure.

Fig. 2 Example decompositions of a graph and the corresponding values of vector x. (a) the original graph with $x = (1,1,1)$, and (b) two component decomposition with $x = (0,0,1)$.

factors, since it is directly related the improved ride and NVH (Noise, Vibration, and Harshness) qualities and crashworthiness [11]. To accurately predict the stiffness of an assembled body structure, Chang [12] used a beam-spring model of BIW where spot-welded joints were modeled as torsional springs. In this work he demonstrated that the model can accurately predict the global deformation of automotive body substructures. Recently, correlation between torsional spring properties of joints and the length of structural member was studied [13] to assess the accuracy of joint model. Kim [14] employed an 8-DOF beam theory for modeling joints to consider the warping and distortion in vibration analysis. However, these works focus on the accurate prediction of the structural behavior of a given assembly (i.e., already "decomposed" structure design) and do not address where to place joints based on the predicted stiffness of an assembly.

3 Approach

This section describes the proposed method for simultaneously identifying the optimal set of components and joint attributes (rates of torsional springs) considering the stiffness of the assembled structure. It is assumed that joints have less stiffness than components and therefore reduce the rigidity of the overall structure.[1] The following steps outline the basic procedure:

1. Given a structure of interest (Fig. 1(a)), define the basic members and potential joint locations (Fig. 1(b)).
2. Construct a structural topology graph $G = (V,E)$ with node set V and edge set E, which represents the connectivity of the basic members defined in step 1 (Fig. 1(c)). A node and an edge in G correspond to a member and a joint, respectively.
3. Obtain the optimal decomposition of G that gives the best structural performance via Genetic Algorithm (Fig. 1(d)), and map the decomposition result back to the original structure (Fig. 1(e)). During optimization, the structural performance of decomposition is evaluated by a Finite Element Method.

3.1 Definition of Design Variables. Since a graph can be decomposed by deleting some edges, a vector $x = (x_i)$ of binary
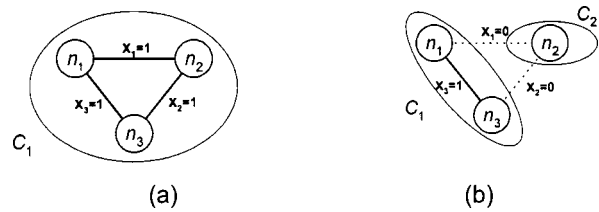
variable x_i can be used to represent a decomposition of structural topology graph G. The dimension of the vector $x = (x_i)$ is equal to the number of the edges $|E|$ in G:

$$\mathbf{x} = (x_1 x_2 \ldots x_1 \ldots x_{|E|-1} x_{|E|}) \tag{1}$$

where

$$x_i = \begin{cases} 1 & \text{if } e_i \text{ exists in the decomposed graph} \\ 0 & \text{otherwise} \end{cases}$$

Figure 2 illustrates example decompositions of a graph and the corresponding values of vector x. Figure 2(a) shows the original graph G without decomposition, where $V = \{n_1, n_2, n_3\}$ and $E = \{e_1, e_2, e_3\}$. Since all edges are present without decomposition, the corresponding vector $\mathbf{x} = (x_1, x_2, x_3)$ is (1,1,1). If vector x takes this value, an entire graph G is interpreted as one component, which is denoted as C_1 in the figure. Similarly, Fig. 2(b) shows a two-component decomposition consisting of components C_1 and C_2 obtained by deleting e_1 and e_2 (indicated as dashed lines) in G. This decomposition can be represented using vector x as $x = (x_1, x_2, x_3) = (0,0,1)$.

Joint attributes are defined as another vector $\mathbf{y} = (\mathbf{y_1}, \mathbf{y_2}, \ldots, \mathbf{y}_{|E|})$, where y_i, $i = 1, 2, \ldots, |E|$ is a n-dimensional vector representing the joint attributes of edge e_i in the structural topology graph. In other words, the joint design at edge e_i is determined by n design variables $\mathbf{y}_i = (y_{i1}, y_{i2}, \ldots, y_{in})$. In the following case studies, joint attribute y_i represents the rates (spring constants) of torsional springs [Nm/rad] of the joint corresponding to edge e_i of the structural topology graph. In the first case study, the 2-dimensional analysis model (side frame decomposition of a passenger car) needs only one design variable (rotation around z axis) for joint design. In this case $n = 1$ and $\mathbf{y}_i = y_i = k_{iz}$. However, in the second case study (under body frame decomposition of a passenger car) we considered 3-dimensional analysis model that requires three design variables (rotations around spring x, y, and z axes) for joint design. In this case $n = 3$ and $\mathbf{y}_i = (k_{ix}, k_{iy}, k_{iz})$. During optimization, the value of $\mathbf{y}_i$ is only considered if $x_i = 0$ when joint between components is required.

3.2 Definition of Constraints. The first constraint for the design variable $\mathbf{x}$ comes from the definition of $\mathbf{x}$. Namely, each element of the vector $\mathbf{x}$ should be 0 or 1:

$$x_i \in \{0,1\} \tag{2}$$

In the current formulation, we assume a desired number of decomposition k is given by the designer, considering this is constrained by the number of available assembly stations.[2] Therefore, the decomposition of G should result in k disconnected subgraphs:

$$\text{N\_COMPONENTS (GRAPH}(\mathbf{x})) = k \tag{3}$$

---

[1]While this is true for many joints such as spot welds, threaded fasteners, and rivets, some joints (e.g., arc welds) can be stiffer than components themselves.

[2]Given a cost model of component manufacturing, it would be possible to include k in the design variable and determine the optimal number of components, which is a part of future investigation.

where GRAPH($\mathbf{x}$) is a function that returns the graph corresponding to the decomposition of G with x, and N_COMPONENTS(G) is a function that returns the number of disconnected subgraphs ("components") in graph.

The third constraint of $\mathbf{x}$ is to ensure the decomposed components are economically manufacturable by given manufacturing means. For example, components with a branched topology would not be economically manufacturable by sheet metal stamping. Also, when we consider 3D structure with stamping process, any decomposed component should be on 2 dimensional plane. Those constraints will be determined by the manufacturing methods and also by the capacity of the machines to be used. The following is a general form of manufacturability constraint:

$$\text{IS\_MANUFACTURABLE (GRAPH ($\mathbf{x}$))} = 1 \qquad (4)$$

where IS_MANUFACTURABLE(G) is a function that returns 1 when all disconnected subgraphs in G are manufacturable by given manufacturing methods, such as stamping of sheet metal, and otherwise returns 0. In the following case studies, it is simply defined as the condition where the bounding boxes of all decomposed components are less than a given size, which represents the upper limit of stamping die size.

Finally, elements of $\mathbf{y}_i$ should simply be among the feasible selections:

$$y_{ij} \in \mathbf{F} \quad i=1,2,\ldots,|E|, \quad j=1,2,\ldots,n \qquad (5)$$

where $\mathbf{F}$ is a set of feasible values of given joint attributes (the rate of torsional spring in the following examples). Assuming that rate of a joint is defined by the type of the joint and the number of welding spots, the value of y_{ij} is chosen among discrete values within the reasonable range of torsional spring rate.

3.3 Definition of Objective Function. A component set specified by vector $\mathbf{x}$ (a set of the node sets of disconnected subgraphs in GRAPH ($\mathbf{x}$)) is evaluated for the stiffness of the assembled structure with the joint attribute specified by $\mathbf{y}$. The stiffness of an assembled structure can be measured as the negative of the sum of displacements at the pre-specified points of the structure for given boundary conditions:

$$\text{stiffness} = -\text{DISPLACEMENTS (GRAPH($\mathbf{x}$),$\mathbf{y}$)} \qquad (6)$$

where DISPLACEMENTS(G,$\mathbf{y}$) is a function that returns the sum (or the maximum) of displacements at the pre-specified points of the assembled structure, computed by finite element methods.

Since we assume the number of components is given, a decomposition would be the stiffest if the maximum spring constant is used at all joints. This corresponds to the situation where the maximum number of spot welds is used for all joints, which is obviously not a very economical solution. It would be of engineering interest, therefore, to find out the optimal balance between the sum of spring constants (a measure of the total number of spot welds) and structural stiffness of the assemble structure. This results in the following objective function (to be maximized) that evaluates stiffness of the structure and also total sum of spring constants in the joints:

$$f(x,y) = C + w_1 \cdot \text{stiffness} - w_2 \sum y_{ij} \qquad (7)$$

where C is a positive constant, stiffness is defined as Eq. (6), w_1 and w_2 are positive weights. The purpose of constant C is to ensure the positive value of fitness for any values of $\mathbf{x}$ and $\mathbf{y}$, required by Genetic Algorithms as stated below. After all, the following optimization model is to be solved:
 maximize $f(\mathbf{x},\mathbf{y})$ (objective function in Eq. (7))
  subject to

$$\text{N\_COMPONENTS (GRAPH ($\mathbf{x}$))} = k$$
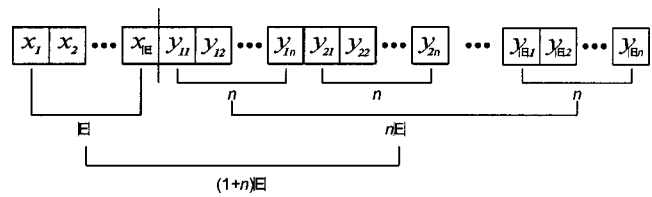
$$\text{IS\_MANUFACTURABLE (GRAPH ($\mathbf{x}$))} = 1,$$

Fig. 3 Chromosome representation of design variables x = (x_i) and y = (y_i), where the elements of these vectors are simply laid out to form a linear chromosome of length (1 + n)*|E|. Note n is the number of design variables that determine the design of one joint.

$$\mathbf{x} = (x_i), \quad x_i \in \{0,1\}, \quad i=1,\ldots,|E|$$
$$\mathbf{y} = (\mathbf{y}_i), \quad y_i = (y_{ij}), \quad y_{ij} \in \mathbf{F}, \quad i=1,\ldots,|E|, \quad j=1,\ldots,n$$

It should be noted that the above optimization model contains a standard k-partitioning problem of an undirected graph [14], and additional nonlinear terms in the objective functions and constraints.

3.4 Genetic Algorithms. Due to the NP-completeness of the underlying graph partitioning problem [15], the above optimization model is solved using Genetic Algorithm (GA). GA is a heuristic optimization algorithm that simulates the process of natural selection in biological evolution [5,6]. The results of the following examples are obtained using a steady-state GA [16], a variation of the "vanilla" GA tailored to prevent premature convergence. Basic steps of a steady-state GA is outlined below [2]:

1. Randomly create a population P of n individuals with chromosomes (a representation of design variable $\mathbf{x}$). Evaluate their fitness values and store the best chromosome. Also create an empty subpopulation Q.
2. Select two chromosomes c_i and c_j in P with probability:

$$\text{Prob}(c_i \text{ is selected}) = \frac{f_i}{\Sigma f_k}$$

where f_i is the fitness value of chromosome c_i.
3. Crossover c_i and c_j to generate two new chromosomes c_i' and c_j'.
4. Mutate c_i' and c_j' with a certain low probability.
5. Evaluate the fitness values of c_i' and c_j'. Add them in Q. If Q contains less than m new chromosomes, go to step 2.
6. Replace m chromosomes in P with m chromosomes in Q. Empty Q. Update the best chromosome and increase the generation counter. If the generation counter has reached a pre-specified number, terminate the process and return the result. Otherwise go to step 2.

In GAs, design variables are represented as a "string" of numbers called chromosomes on which genetic operators such as crossover and mutation are performed. The components of our two design variables $\mathbf{x} = (x_i)$ and $\mathbf{y} = (y_i)$ are simply laid out as $x_1,x_2,\ldots,x_{|E|},y_{11},y_{12},\ldots,y_{1n},y_{21},y_{22},\ldots,y_{2n},\ldots,y_{|E|1}, y_{|E|2},\ldots,y_{|E|n}$ in a linear chromosome of length $(1+n)*|E|$ as illustrated in Fig. 3. Two-point crossover is used where the crossover sites are selected to ensure a cut in both $\mathbf{x}$ and $\mathbf{y}$ portions of the chromosome.

Since we have formulated the optimization model as a maximization problem, the fitness values of a chromosome can be computed from the corresponding values of the design variables $\mathbf{x}$ and $\mathbf{y}$ as:

$$\text{fitness} = f(\mathbf{x},\mathbf{y}) - \text{penalty} \qquad (8)$$

where penalty is defined as:

$$\text{penalty} = w_3(\text{N\_COMPONENTS } (\text{GRAPH } (\mathbf{x})) - k)^2$$

$$+ w_4(\text{IS\_MANUFACTURABLE } (\text{GRAPH } (\mathbf{x})) - 1)^2$$

$$(9)$$

where w_3, w_4 are positive weights. After all, the fitness function looks like:

$$\text{fitness} = C - w_1 \cdot \text{DISPLACEMENTS } (\text{GRAPH } (\mathbf{x}), \mathbf{y}) - w_2$$

$$\cdot \sum y_i - w_3(\text{N\_COMPONENTS } (\text{GRAPH } (\mathbf{x})) - k)^2$$

$$- w_4(\text{IS\_MANUFACTURABLE } (\text{GRAPH } (\mathbf{x})) - 1)^2$$

$$(10)$$

As stated earlier, computing DISPLACEMENTS(G,$\mathbf{y}$) requires finite element methods and is the most time consuming part among the above four terms in the fitness function. To improve the runtime efficiency, we have devised a database to store each FEM result with the corresponding value of chromosome during a GA run. When a chromosome is evaluated, the algorithm first looks into the datable for the same chromosome value. If there is a match, it simply retrieves the pre-computed FEM result and skips the FEM analysis.

4 Case Studies

In this section, the assembly synthesis method described in the previous section is applied to a side frame of a four-door sedan type passenger car (Fig. 4) and an under body frame of a passenger car (Fig. 5). In both case studies, spot-welded joints are considered as joining methods and are modeled as torsional springs in the analysis model.

Figure 6 shows the flowcharts of the implemented software for the case studies. During the fitness calculation (Fig. 6(b)), the software generates the input file for a FEM solver, run the FEM solver, and retrieves the necessary data within the output file. The
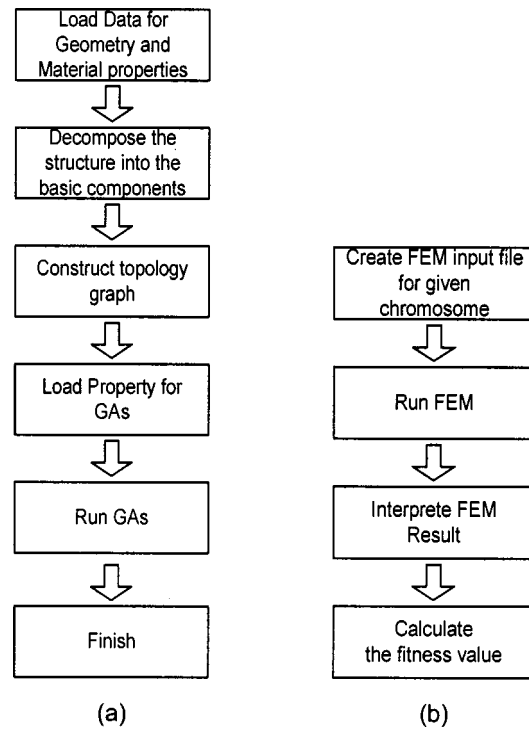
Fig. 6 Flowchart of optimal decomposition software. (a) overall flow, and (b) fitness calculation.

software is written in C++ program using LEDA[3] libraries. GAlib[4] and ABAQUS[5] are used as a GA optimizer and a FEM solver, respectively.

4.1 Case Study 1: Side Frame Decomposition of a Four-Door-Sedan Type Passenger Car. The following assumptions are made according to Chang [12]: 1) the side frame is subject to a static bending due to weight of the vehicle, 2) the frame can be modeled as a two dimensional structure, and 3) its components are joined with spot welds modeled as torsional springs, whose axis of rotation is perpendicular to the plane on which the frame lies.

4.1.1 Structural Model. Figures 7 and 8 show the 9 basic members defined on the side frame in Fig. 4, and the resulting structural topology graph, respectively. Each basic member was modeled as a beam element with a constant cross section, whose properties (area and moment of inertia) are listed in Table 1, which are calculated from the body geometry of a typical passenger car. Each intersecting member in the frame is assumed to be of constant cross section up to the intersection of the axis of the members. This will reduce the connection among multiple beams to be represented as a point [12], and hence allows to model a joint as a torsional spring around the point.

Due to the complex geometry, residual stresses, and friction between the mating surfaces, the detailed structural modeling of spot welded joints are quite difficult [12]. It is a standard industry practice, therefore, to model spot-welded joints as torsional springs, whose spring rates [Nm/rad] are empirically obtained though experiments or detailed FEM analyses. In the following case studies, the rates of the torsional springs at each joint in a decomposition (vector $\mathbf{y}$ in Eq. (10)) are regarded as:

- Case 1-1: constants in Table 2.
- Case 1-2: variables between 0.01×10^6 and 0.20×10^6 [Nm/rad].
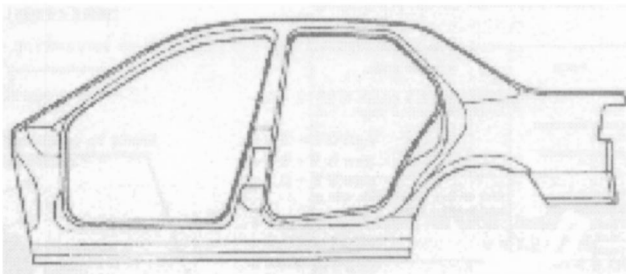

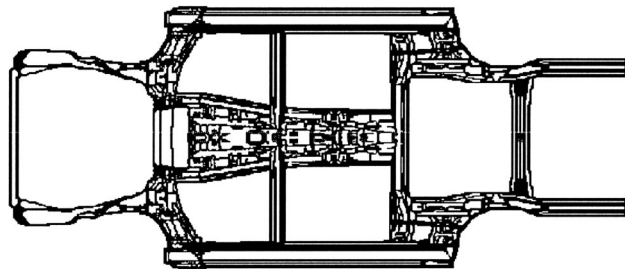Fig. 4 A side frame of a passenger car used in Case Study 1 (adopted from [17] with authors' permission)

Fig. 5 An under body frame of a passenger car used in Case Study 2 (adopted from [17] with authors' permission)
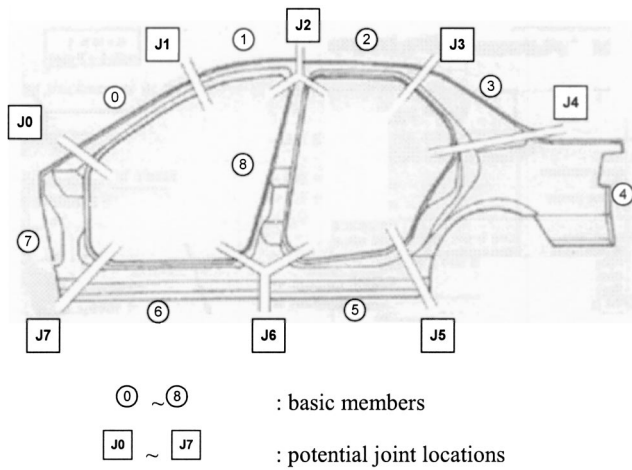
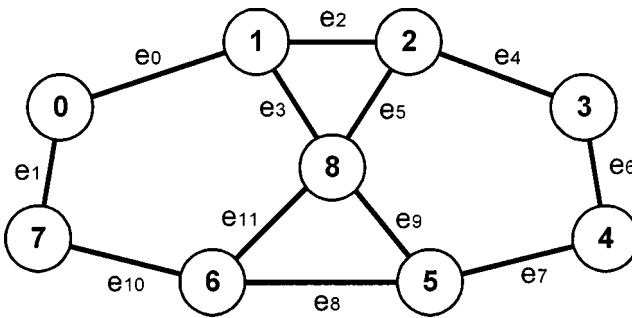**Fig. 7 Definition of basic members and potential joint locations of side frame structure**

Fig. 8 Structural topology graph of the side frame, with nodes 0~7 represent basic members, and edges $e_0 \sim e_{11}$ represent potential joints between two basic members

In other words, in Case 1-1 vector **x** in Eq. (10) is the only design variable and vector **y** is treated as a constant, whereas in Case 1-2 both **x** and **y** are design variables. Since the set of feasible spring rate $\mathbf{F} = \{y | 0.01 \times 10^6 \leq y \leq 0.20 \times 10^6\}$ in Case 1-2 contains all values in Table 2, the optimization model in Case 1-2 is a relaxation of the one in Case 1-1.

4.1.2 Boundary Conditions. The structure was assumed to be placed on a simple support system consisting of a pair of hinge supports at the front body mount location and a pair of roller supports at the mount locations near the rear locker pillar as shown in Fig. 9. The loading condition of the static bending strength requirement is considered, where the downward loading is the weight of a passenger car (10,000 [N]).

Table 1 Cross-sectional properties of basic members in Fig. 6, calculated from typical passenger vehicle body geometry [17]

No.	Nomenclature	Cross-sectional area [m²]	Moment of inertia [m⁴]
0	Windshield Pillar	3.855×10^{-4}	1.860×10^{-7}
1	Front Roof Rail	4.789×10^{-4}	5.411×10^{-7}
2	Rear Roof Rail	4.789×10^{-4}	5.411×10^{-7}
3	C Pillar	12.840×10^{-4}	9.967×10^{-7}
4	Rear Wheel House	7.840×10^{-4}	9.342×10^{-7}
5	Rear Rocker	20.730×10^{-4}	8.792×10^{-7}
6	Front Rocker	20.730×10^{-4}	8.792×10^{-7}
7	Hinge Pillar	10.369×10^{-4}	12.784×10^{-7}
8	Center Pillar	5.443×10^{-4}	1.625×10^{-7}

Table 2 Torsional spring rates of the joints in side frame of a typical passenger vehicle [17]

No.	Joint location	Joint rate [Nm/rad]
J0	Hinge Pillar and Windshield Pillar	0.20×10^6
J1	Windshield Pillar and Front Roof Rail	0.01×10^6
	Front and Rear Roof Rails	0.01×10^6
J2	Rear Roof Rails, and Center Pillar	0.01×10^6
	Front Roof Rails, and Center Pillar	0.01×10^6
J3	Rear Roof Rail and C Pillar	0.01×10^6
J4	C Pillar and Rear Weal House	0.20×10^6
J5	Rear Weal House and Rear Rocker	0.20×10^6
	Front and Rear Rocker	0.20×10^6
J6	Rear Rocker and Center Pillar	0.20×10^6
	Front Rocker and Center Pillar	0.20×10^6
J7	Hinge Pillar and Front Rocker	0.20×10^6

4.1.3 Measure of Structural Stiffness and Manufacturability of Components. Under normal loading conditions, the front door frame should retain its original shape to guarantee the normal door opening and closing. Based on this consideration, DISPLACEMENTS $(G, \mathbf{y})$ in Eq. (10) is defined as:

$$\text{DISPLACEMENTS } (G, \mathbf{y}) = \max\{\overline{A1A2}, \overline{B1B2}\} \qquad (11)$$

where

$A1$ = upper right corner of the front door frame after deformation.

$A2$ = upper right corner of the front door without deformation, attached to the deformed hinge.

$B1$ = lower right corner of the front door frame after deformation.

$B2$ = lower right corner of the front door without deformation, attached to the deformed hinge.

Points $A1$, $A2$, $B1$, and $B2$ are illustrated in Fig. 10. The locations of $A1$ and $B1$ are obtained directly from the FEM results. The following assumptions are made on the locations of $A2$ and $B2$:

- The door only rotates around a point O in Fig. 10. The angle of rotation is defined as the angle between $\overline{OP0}$ and $\overline{OP1}$. $\overline{OP0}$ represents the hinge without deformation, whereas $\overline{OP1}$ represents the deformed hinge.
- The front door is a rigid body: Deformation of the door due to the external loading is negligible compared to the one of the frame (i.e., the door is a "rigid body").

4.1.4 Decomposition Results. As a base line for comparing the effect of the joints, we first examined one piece structure with
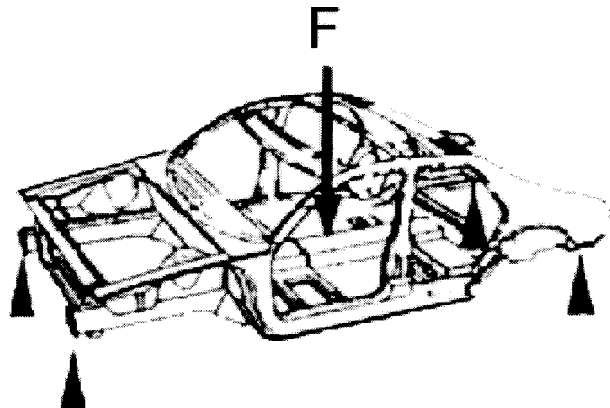

Fig. 9 Loading condition of basic bending requirement. Loading F=10,000 [N], which is the weight of a typical passenger vehicle [17].
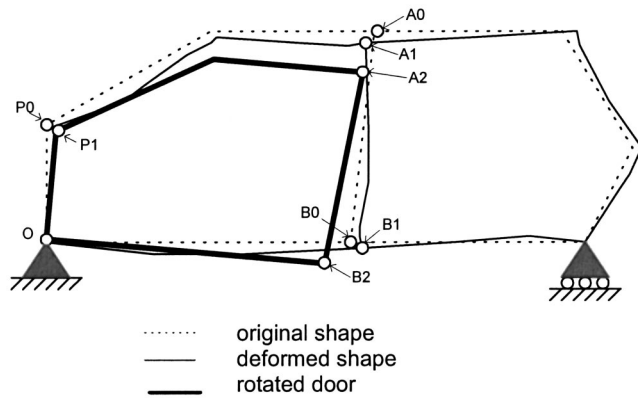
Fig. 10 Definition of DISPLACEMENTS (G, y) used in Case Study 1. Overall displacement of side frame is max$\{d_1, d_2\}$, where d_1 and d_2 are the displacements of upper and lower right corners of the door, respectively, measured with respect to un-deformed door geometry attached to deformed hinge OP1.

no joints and the fully decomposed structure made of the 9 basic members with the 8 joints defined in Fig. 7. The joint rates in Table 2 are used for the FEM analysis of the fully decomposed structure. Since the joints are less stiff than the material of the basic members, it is expected that the fully decomposed structure exhibits a larger value of DISPLACEMENTS$(G, \mathbf{y})$ as defined in Fig. 10, than the one piece structure. Figures 11 and 12 show the FEM results of the one-piece structure and the fully-decomposed structure, respectively. As expected, the existence of joints causes a significant increase in the amount of DISPLACEMENTS in the structure, as well as much difference in the deformed shapes. The value of DISPLACEMENTS of the fully decomposed structure (Fig. 12) is about 6 times larger than that of the one piece struc-
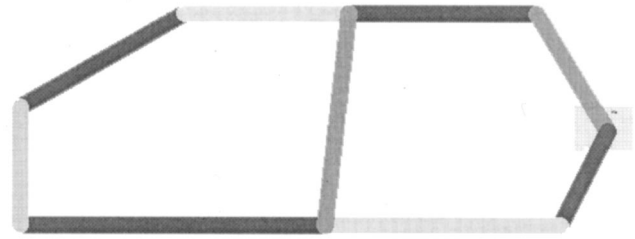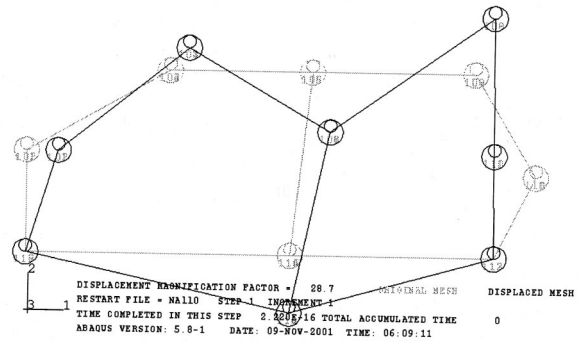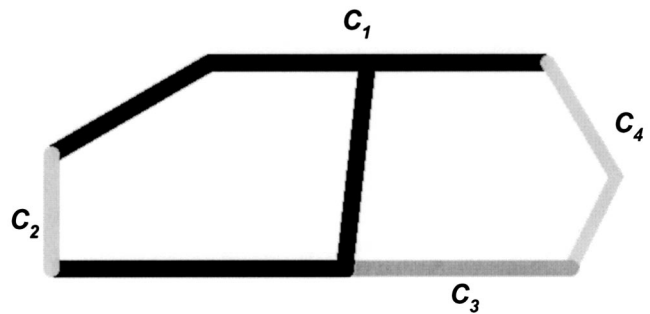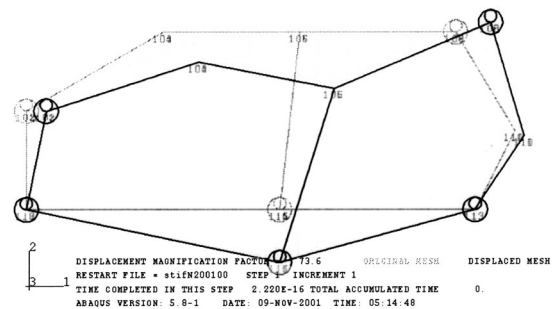

Fig. 12 Baseline result. (a) fully decomposed structure ($k=9$) and (b) its deformation with DISPLACEMENTS=8.251 [mm].
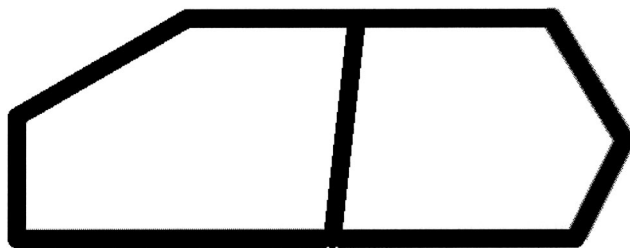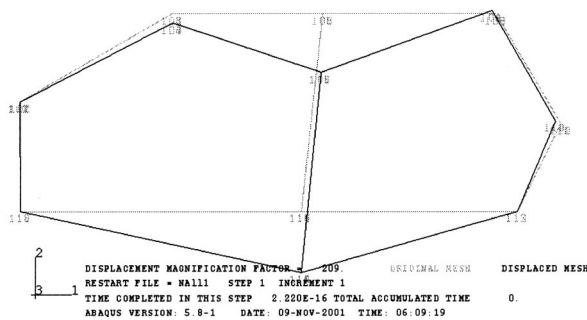
Fig. 11 Baseline result. (a) one piece structure ($k=1$) and (b) its deformation with DISPLACEMENTS=1.411 [mm].
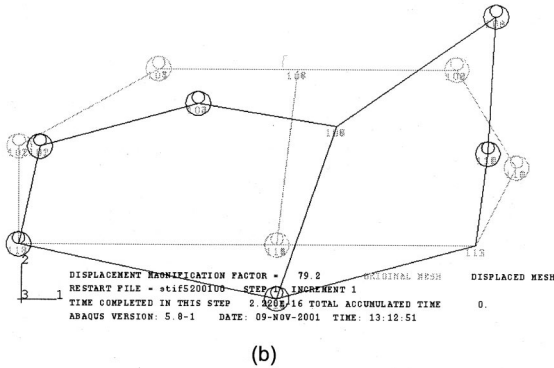

Fig. 13 4-component decomposition ($k=4$) with constant joint rates in Table 2 (Case 1-1). (a) optimal decomposition and (b) its deformation with DISPLACEMENTS=0.075 [mm]. C_i in (a) indicates i-th component.
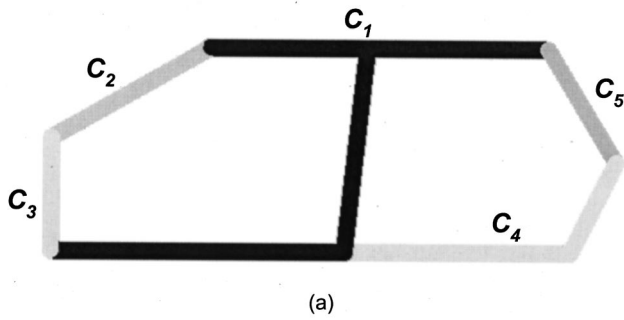
Fig. 14 5-component decomposition ($k=5$) with constant joint rates in Table 2 (Case 1-1). (a) optimal decomposition and (b) its deformation with DISPLACEMENTS=0.109 [mm]. C_i in (a) indicates i-th component.

Fig. 15 4-component decomposition ($k=4$) with variable joint rates (Case 1-2). (a) optimal decomposition and (b) its deformation with DISPLACEMENTS=0.062 [mm]. The number at each joint in (a) indicates the optimal joint rate in [10^4 Nm/rad]. C_i in (a) indicates i-th component.
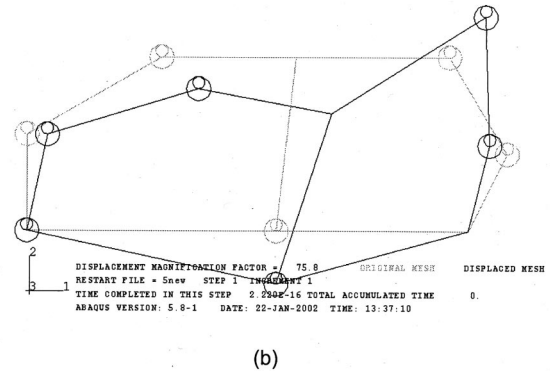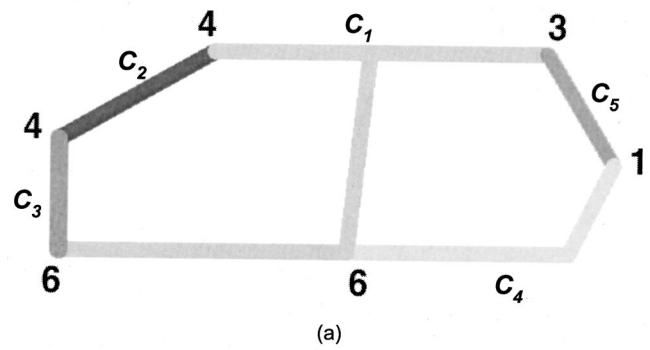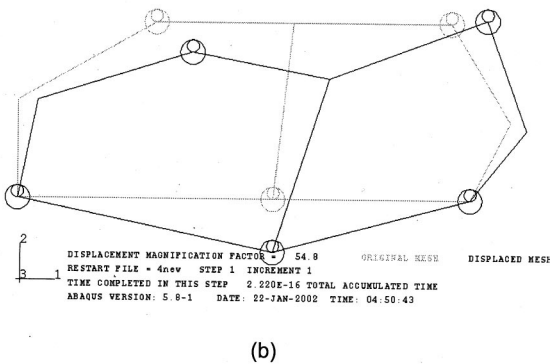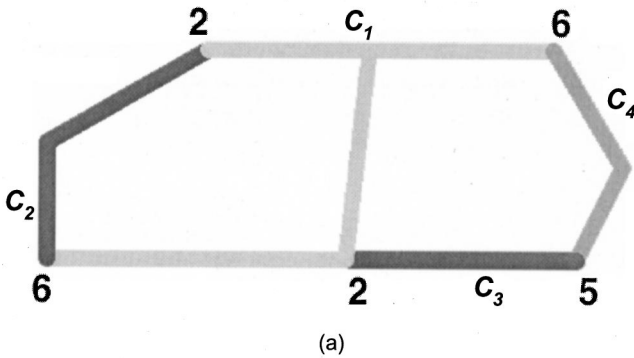

Fig. 16 5-component decomposition ($k=5$) with variable joint rates (Case 1-2). (a) optimal decomposition and (b) its deformation with DISPLACEMENTS=0.065 [mm]. The number at each joint in (a) indicates the optimal joint rates in [10^4 Nm/rad]. C_i in (a) indicates i-th component.

ture (Fig. 11). However, even the one piece structure does not fully retain the original shape of the front door, resulted in a fairly large value of DISPLACEMENTS=1.411 [mm].

Next, the structure is decomposed to 4 and 5 components, each with constant joint rates in Table 2 (Case 1-1) and variable joint rates between 0.01×10^6 and 0.20×10^6 [Nm/rad] (Case 1-2). Figures 13 and 14 show the 4- and 5-component optimal decompositions with constant joint rates (Case 1-1), respectively. Figures 15 and 16 show the 4- and 5-component optimal decompositions with variable joint rates (Case 1-2), respectively. Table 3 shows a summary of the results of the case studies including the base line cases. The following GA parameters are used in these results:

- number of population=200.
- number of generation=100 (Case 1-1); 200 (Case 1-2).
- replacement probability=0.50.
- mutation probability=0.001 (Case 1-1); 0.10 (Case 1-2).
- crossover probability=0.90.

Table 3 Summary of results. Note that all optimization results produce better DISPLACEMENTS than no decomposition and full decomposition cases. For both $k=4$ and 5, Case 1-2 exhibits better DISPLACEMENTS with less total joint rate (hence less weld spots) than Case 1-1.

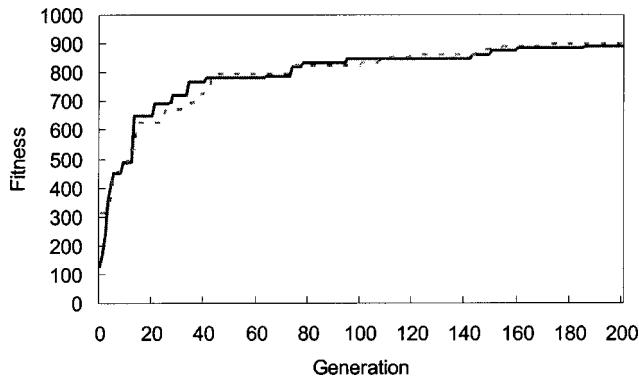| Case	DISPLACEMENTS [mm]	Total joint rate [Nm/rad]
No decomposition (Figure 11)	1.411	0.00×10^6
Full decomposition (Figure 12)	8.251	1.03×10^6
Case 1-1, $k=4$ (Figure 13)	0.075	0.81×10^6
Case 1-1, $k=5$ (Figure 14)	0.109	0.82×10^6
Case 1-2, $k=4$ (Figure 15)	0.062	0.21×10^6
Case 1-2, $k=5$ (Figure 16)	0.065	0.24×10^6

Fig. 17 Evolution history of two typical cases. The solid line indicates the history of 4-component decomposition ($k=4$) with variable joint rates, and the dotted line indicates the 5-component decomposition ($k=5$) with variable joint rates. The fitness value converges approximately after 200 generations, which is used as the termination criterion (Case 1-2).
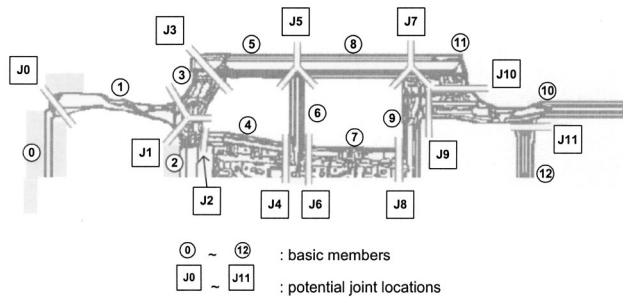

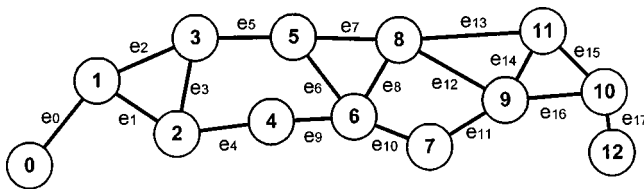**Fig. 18 Definition of basic members and potential joint locations of under body frame structure**

Fig. 19 Structural topology graph of the under body side frame, with nodes 0~12 represent basic members, and edge e0~e17 represent potential joints between two basic members

The evolution history of two typical cases (Case 1-2, 4 and 5 components) in Fig. 17 shows that the above GA parameters gave us satisfactory convergence in the fitness value calculated from Eq. (10).

The decomposition results in Fig. 13–16 indicate that the structure is decomposed to a desired number of components and the front door frames after deformation preserve their original shape fairly well. In fact, all 4- and 5- component decompositions resulted in the smaller values of DISPLACEMENTS than the one piece structure in Fig. 11. This is due to the fact that rear door frame (basic members 2, 3, 4 and 5) "absorbs" the deformation due to the external loads by having relatively less stiff joints. All the optimized shapes show no joints between Front and Rear Roof Rails (basic members 1 and 2) and Center Pillar (basic member 8) and between Front Rocker (basic member 6) and Center Pillar (basic member 8). These two positions seem to be critical to preserve the shape of the front door frame against the external loads.

Table 3 reveals that Case 1-2 exhibits smaller DISPLACEMENTS with less total joint rate (hence less weld spots) than Case 1-1 for both $k=4$ and 5. This means, for the same frame design, one can achieve a superior performance (less distortion of the front door frame geometry) with less manufacturing efforts (less number of weld spots). In reality, of course, the distortion of the front door geometry is one of the many criteria which an automotive body structure must satisfy, and hence one cannot simply draw a conclusion that the conventional joints are over designed from these results. As stated earlier, the optimization model of Case 1-2 is a relaxation of the one of Case 1-1. Therefore, the optimal solutions of Case 1-2 must be at least as better as the ones in Case 1-1, which is shown in Table 3.

4.2 Case Study 2: Under Body Frame Decomposition of a Passenger Car. The following assumptions are made to model this case study: 1) under body frame structure is to be optimized to minimize the longitudinal twist angle under the longitudinal torsion, 2) the frame can be modeled as a three dimensional symmetric beam structure, 3) due to the symmetric nature of the under body frame, right half of the under body frame will be decomposed and optimized. The other half side of the under body frame will have the same structure as the right side, and 4) components of under body frame are joined with spot welds modeled as three torsional springs whose axes of rotations are parallel to the 3 axes in global Cartesian coordinate system.

4.2.1 Structural Model. Using the symmetric nature of the under body frame, the right half of the under body frame is decomposed. Figures 18 and 19 show the 13 basic members defined on the right half of the under body frame in Fig. 5 and the resulting structural topology graph, respectively. As in Case Study 1,

Table 4 Cross-sectional properties of basic members in Fig. 18, calculated from typical body geometry [16]

No.	Nomenclature	Cross-sectional area [m²]	Moment of inertia I_{11} [m⁴]	Moment of inertia I_{22} [m⁴]	Torsional Rigidity J [m⁴]
0	Front Cross Member	3.60×10^{-4}	5.000×10^{-7}	1.800×10^{-7}	6.800×10^{-7}
1	Front Frame Rail	8.83×10^{-4}	20.500×10^{-7}	2.780×10^{-7}	23.300×10^{-7}
2	Middle Cross Member 1	8.67×10^{-4}	11.500×10^{-7}	6.960×10^{-7}	23.300×10^{-7}
3	Front Torque Box	9.90×10^{-4}	14.800×10^{-7}	6.190×10^{-7}	13.100×10^{-7}
4	Mid Rail 1	6.17×10^{-4}	6.080×10^{-7}	3.490×10^{-7}	9.570×10^{-7}
5	Frame Side Rail 1	8.75×10^{-4}	22.400×10^{-7}	1.525×10^{-7}	37.700×10^{-7}
6	Middle Cross Member 2	9.90×10^{-4}	14.800×10^{-7}	6.190×10^{-7}	13.100×10^{-7}
7	Mid Rail 2	6.17×10^{-4}	6.080×10^{-7}	3.490×10^{-7}	9.570×10^{-7}
8	Frame Side Rail 2	8.75×10^{-4}	22.400×10^{-7}	1.525×10^{-7}	37.700×10^{-7}
9	Middle Cross Member 3	9.90×10^{-4}	14.800×10^{-7}	6.190×10^{-7}	13.100×10^{-7}
10	Rear Frame Stub	6.17×10^{-4}	6.080×10^{-7}	3.490×10^{-7}	9.570×10^{-7}
11	Rear Torque Box	15.90×10^{-4}	24.800×10^{-7}	9.190×10^{-7}	53.100×10^{-7}
12	Rear Cross Member	9.90×10^{-4}	14.800×10^{-7}	6.190×10^{-7}	13.100×10^{-7}

Table 5 Torsional spring rates of the joints in under body frame of a passenger car from typical passenger car body model [17]. Here, x, y, z directions are along the length, width and height of the passenger car, respectively.

No.	Joint location	Joint rate [Nm/rad]		
		x direction	y direction	z direction
J0	Front Cross Member and Front Frame Rail	0.004×10^6	0.002×10^6	0.004×10^6
	Front Frame Rail and Middle Cross Member 1	0.045×10^6	0.002×10^6	0.008×10^6
J1	Middle Cross Member 1 and Front Torque Box	0.184×10^6	0.065×10^6	0.184×10^6
	Front Torque Box and Front Frame Rail	0.179×10^6	0.043×10^6	0.147×10^6
J2	Middle Cross Member 1 and Mid Rail 1	0.045×10^6	0.002×10^6	0.008×10^6
J3	Front Torque Box and Frame Side Rail 1	0.004×10^6	0.002×10^6	0.004×10^6
J4	Mid Rail 1 and Middle Cross Member 2	0.045×10^6	0.002×10^6	0.008×10^6
	Frame Side Rail 1 and Middle Cross Member 2	0.179×10^6	0.043×10^6	0.147×10^6
J5	Middle Cross Member 2 and Frame Side Rail 2	0.045×10^6	0.002×10^6	0.008×10^6
	Frame Side Rail 2 and Frame Side Rail 1	0.184×10^6	0.065×10^6	0.184×10^6
J6	Middle Cross Member 2 and Mid Rail 2	0.045×10^6	0.002×10^6	0.008×10^6
	Frame Side Rail 2 and Middle Cross Member 3	0.179×10^6	0.043×10^6	0.147×10^6
J7	Middle Cross Member 3 and Rear Torque Box	0.045×10^6	0.002×10^6	0.008×10^6
	Rear Torque Box and Front Side Rail 2	0.184×10^6	0.007×10^6	0.184×10^6
J8	Mid Rail 2 and Middle Cross Member 3	0.045×10^6	0.002×10^6	0.008×10^6
J9	Middle Cross Member 3 and Rear Frame Stub	0.045×10^6	0.002×10^6	0.008×10^6
J10	Rear Torque Box and Rear Frame Stub	0.002×10^6	0.045×10^6	0.008×10^6
J11	Rear Frame Stub and Rear Cross Member	0.002×10^6	0.045×10^6	0.008×10^6

each basic member is modeled as a beam element with a constant cross section, whose properties (area, moment of inertia and torsional rigidity) are listed in Table 4, calculated from the body geometry of a typical passenger car [17].

As in the previous Case Study, the rates of the torsional springs at each joint in a decomposition (vector $\mathbf{y}$ in Eq. (10)) are regarded as following two cases:

- Case 2-1: constants in Table 5.
- Case 2-2: variables between 0.001×10^6 and 0.20×10^6 [Nm/rad].

In Case 2-1 vector $\mathbf{x}$ in Eq. (10) is the only design variable and vector $\mathbf{y}$ is treated as a constant, whereas in Case 2-2 both $\mathbf{x}$ and $\mathbf{y}$ are design variables. Since the set of feasible spring rate $\mathbf{F} = \{y | 0.001 \times 10^6 \leq y \leq 0.2 \times 10^6\}$ in Case 2-2 contains all values in Table 5, the optimization model in Case 2-2 is a relaxation of the one in Case 2-1.

4.2.2 Boundary Conditions. Pure torsion condition was considered as loading condition. Torsion loading case occurs when only one wheel on an axle strikes a bump. A pure torsion load case is important because it generates very different internal loads in the vehicle structure from the bending load case, and, as such, is a different structural design case. The structure was assumed to be constrained by a pair of hinge supports at the mount location near the both ends of Rear Frame Stub as shown in Fig. 20. Applied
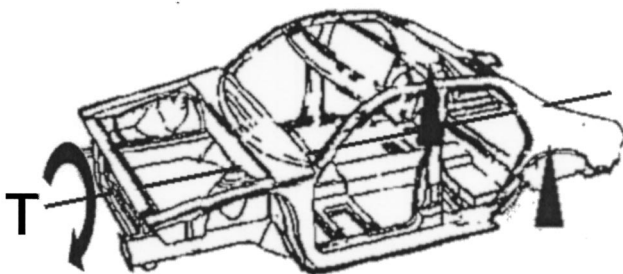

Fig. 20 Loading condition of torsion load case. Applied torque value T is 3750 [Nm] assuming the static wheel reaction in the pure torsion analysis case (Eq. (12)) [17].

torque is calculated as in following equation [18]:

$$\text{Torque} = P_{AXLE} \frac{B}{2} = (\text{Weight in front axle}) \times \frac{(\text{Track of vehicle})}{2} \tag{12}$$

Specific values of a passenger car, $P_{AXLE} = 5{,}000$ [N], and $B = 1.5$ [m], yield Torque $= 3{,}750$ [Nm]. This value is used in the following results.

4.2.3 Measuring of Structural Stiffness and Manufacturability of Components. In this Case Study, the structural stiffness will be the torsional stiffness of the under body frame. Based on this consideration, DISPLACEMENTS$(G, \mathbf{y})$ in Eq. (10) is defined as:

$$\text{DISPLACEMENTS } (G, \mathbf{y})$$
$$= \phi = \frac{\Delta h}{w}$$
$$= \frac{(\text{vertical } dis \tan ce \, btw \ P_1 \quad \text{and} \quad Q_1)}{(\text{width of frame})} \tag{13}$$

where
$P1 =$ Left front corner of the under body frame after deformation.
$Q1 =$ Right front corner of the under body frame after deformation.
$w =$ Width of under body frame.
Points P0, P1, Q0, and Q1 are illustrated in Fig. 21. The locations of $P1$ and $Q1$ are obtained directly from the FEM results.

4.2.4 Decomposition Results. As in the Case Study 1, we first examined one piece structure with no joints and the fully decomposed structure made of the 13 basic members with the 12 joints defined in Fig. 18. The joint rates in Table 5 are used for the FEM analysis of the fully decomposed structure. Since the joints are less stiff than the material of the basic members, it is expected that the fully decomposed structure exhibits a larger value of DISPLACEMENTS(G, y) as defined in Fig. 21, than the one piece structure. Figures 22 and 23 show the FEM results of the one-piece structure and the fully-decomposed structure, respectively. As expected, the existence of joints causes a significant increase in the amount of DISPLACEMENTS in the structure. The value of DISPLACEMENTS of the fully decomposed structure (Fig. 23) is about 3 times larger than that of the one piece structure (Fig. 22).
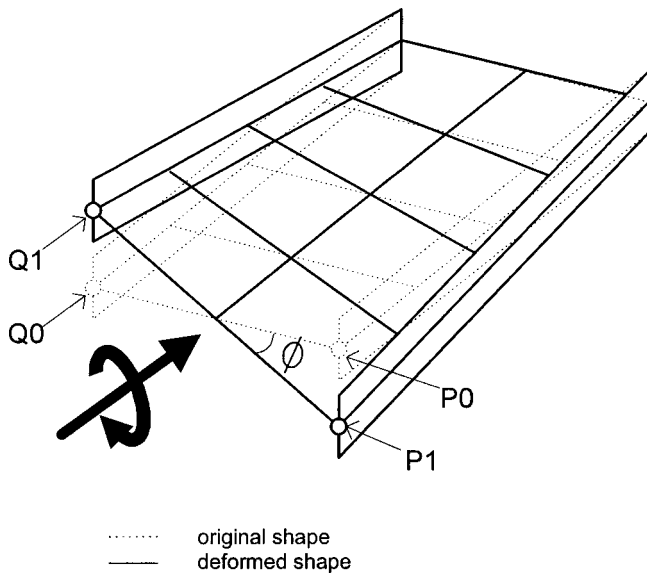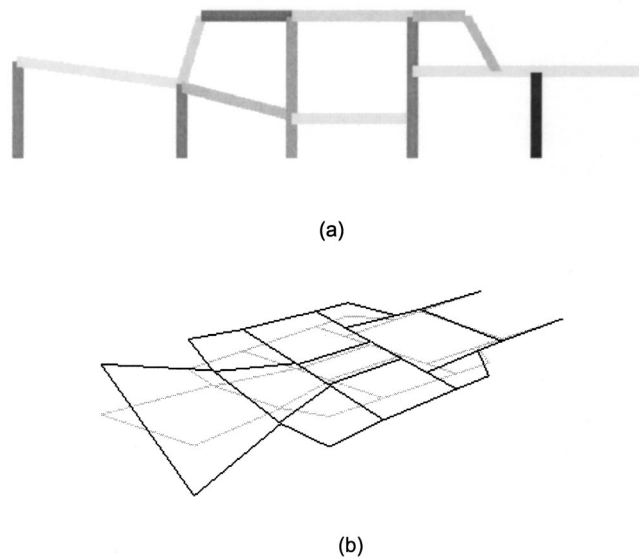
Fig. 23 Baseline result. (a) fully decomposed structure (*k* =13) and (b) its deformation with DISPLACEMENTS=0.9825 [rad].

Fig. 21 Definition of DISPLACEMENTS(*G, y*) used in Case Study 2. Overall displacement of under body frame is $\phi=\Delta h/w$, where Δh and *w* are the vertical distance between P1 and Q1 and width of under body frame, respectively.

The evolution history of two typical cases (Case 2-2, 6 components and 7 components) in the Fig. 28 shows that the above GA parameters gave us satisfactory convergence in the fitness value calculated from Eq. (10).

Next, the structure is decomposed to 6 and 7 components, each with constant joint rates in Table 5 (Case 2-1) and variable joint rates between 0.001×10^6 and 0.20×10^6 [Nm/rad] (Case 2-2). Figures 24 and 25 show the 6- and 7-component optimal decompositions with constant joint rates (Case 2-1), respectively. Figures 26 and 27 show the 6- and 7-component optimal decompositions with variable joint rates (Case 2-2), respectively. Table 6 shows a summary of the results of the Case Study 2 including the base line cases. The following GA parameters are used in these results:

The decomposition results in Figs. 24–27 indicate that the structure is decomposed to a desired number of components. Here, the one piece structure in Fig. 22 resulted in the smallest value of DISPLACEMENTS than the other decomposition cases. This is due to the fact that introducing the joint that is less stiff than the original structure will results in decreased torsional stiffness of the entire structure. However, producing complex structure like this under body frame in one piece is difficult to meet the common manufacturing method with reasonable manufacturing cost. All the optimized shapes show less joints in the outer frame than inner frames. This result implies that the joints in the outer structure
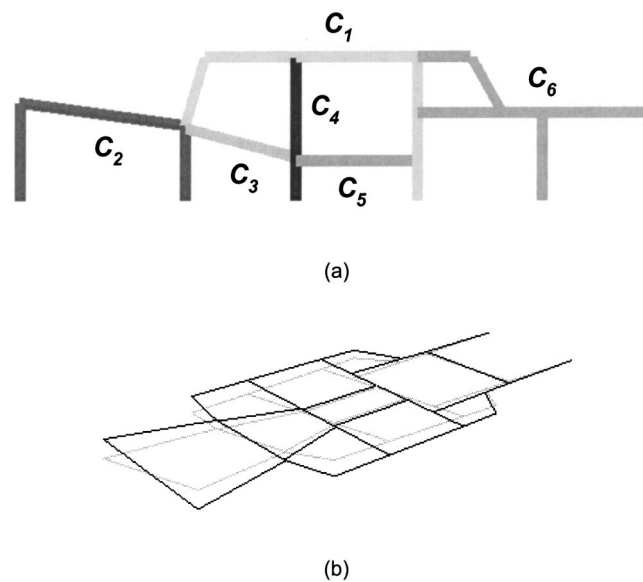
- number of population=100 (Case 2-1); 300 (Case 2-2).
- number of generation=100 (Case 2-1); 200 (Case 2-2).
- replacement probability=0.50.
- mutation probability=0.10.
- crossover probability=0.90.

Fig. 24 6-component decomposition (*k*=6) with constant joint rate in Table 6 (Case 2-1). (a) optimal decomposition and (b) its deformation with DISPLACEMENTS=0.3724 [rad]. C_i in (a) indicates *i*-th component.

Fig. 22 Baseline result. (a) one piece (*k*=1) structure and (b) its deformation with DISPLACEMENTS=0.3488 [RAD].
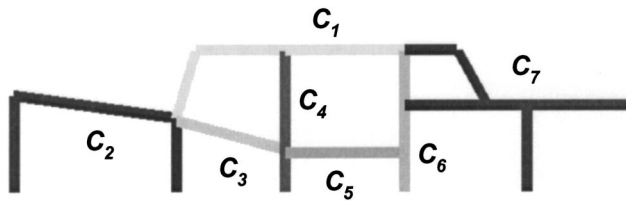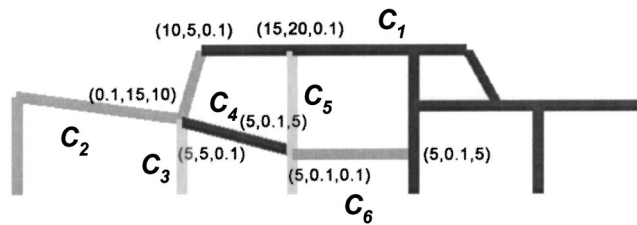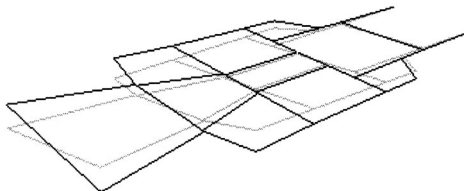
(a)
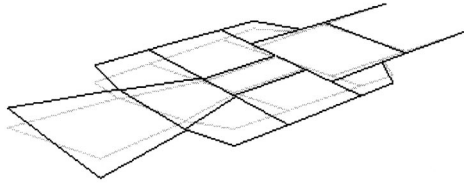
(b)

Fig. 25 7-component decomposition ($k=7$) with constant joint rate in Table 6 (Case 2-1). (a) optimal decomposition and (b) its deformation with DISPLACEMENTS=0.3825 [rad]. C_i in (a) indicates i-th component.

will result in higher DISPLACEMENTS (higher distortion) than the joints near the longitudinal axis of the under body frame.

Table 6 reveals that Case 2-2 exhibits smaller DISPLACEMENTS with less total joint rate (hence less weld spots) than Case 2-1 for both $k=6$ and 7. This means, as discussed in the previous Case Study 1, one can achieve a superior performance (less distortion in the under body frame) with less manufacturing efforts (less number of weld spots) for the same frame design. In reality, of course, the distortion of the under body frame due to the torque
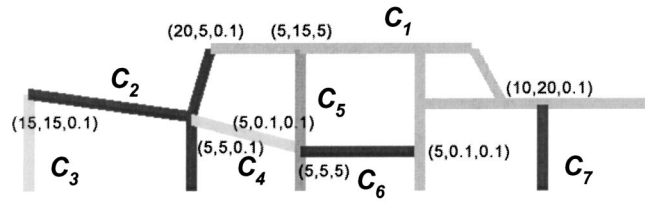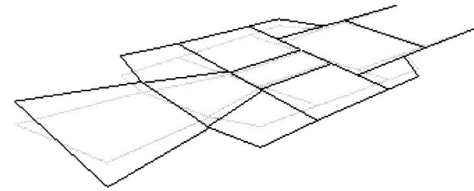

(a)

(b)

Fig. 26 6-component decomposition ($k=6$) with variable joint rates (Case 2-2). (a) optimal decomposition and (b) its deformation with DISPLACEMENTS=0.3696 [rad]. The value at each joint in (a) indicates the optimal joint rate (k_x, k_y, k_z) in [10^4 Nm/rad]. C_i in (a) indicates i-th component.

(a)

(b)

Fig. 27 7-component decomposition ($k=7$) with variable joint rates (Case 2-2). (a) optimal decomposition and (b) its deformation with DISPLACEMENTS=0.3724 [rad]. The value at each joint in (a) indicates the optimal joint rate (k_x, k_y, k_z) in [10^4 Nm/rad]. C_i in (a) indicates i-th component.
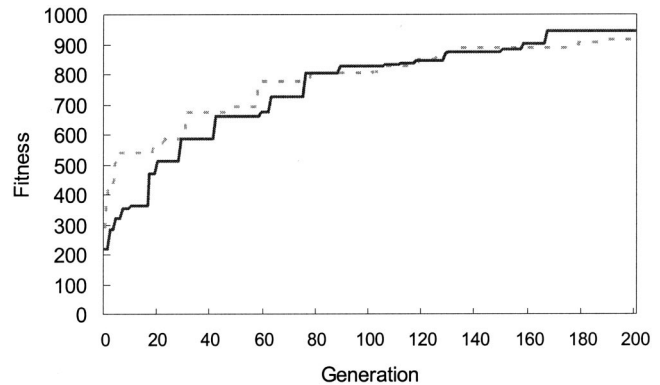

Fig. 28 Evolution history of two typical cases. The solid line indicates the history of 6-component decomposition ($k=6$) with variable joint rates, and the dotted line indicates the 7-component decomposition ($k=7$) with variable joint rates. The fitness value converges approximately after 200 generations, which is used as the termination criterion (Case 2-2).

Table 6 Summary of results. Note that all optimization results produce better DISPLACEMENTS than full decomposition cases. For both $k=6$ and 7, Case 2-2 exhibits better DISPLACEMENTS with less total joint rate (hence less weld spots) than Case 2-1.

Case	DIS-PLACEMENTS [rad]	Total joint rate [Nm/rad]
No decomposition (Figure 22)	0.3488	0.000×10^6
Full decomposition (Figure 23)	0.9825	5.959×10^6
Case 2-1, $k=6$ (Figure 24)	0.3724	2.627×10^6
Case 2-1, $k=7$ (Figure 25)	0.3825	3.594×10^6
Case 2-2, $k=6$ (Figure 26)	0.3696	2.118×10^6
Case 2-2, $k=7$ (Figure 27)	0.3725	2.916×10^6

along the longitudinal axis of the frame is one of the many criteria which an automotive body structure must satisfy, and hence one cannot simply draw a conclusion that the conventional joints are over designed from these results. Again, as stated earlier, the optimization model of Case 2-2 is a relaxation of the one of Case

2-1. Therefore, the optimal solutions of Case 2-2 must be at least as better as the ones in Case 2-1, which is shown in Table 6.

5 Summary and Future Work

This paper described a method for optimally decomposing a structural product based on the stiffness of the end product after assembly. A structure is represented by a graph of its topology, and the optimal decomposition is obtained by combining FEM analyses with a Genetic Algorithm. As the first case study, the side frame of a passenger car is decomposed for the minimum distortion of the front door panel geometry. As the second case study, the under body frame of a passenger car is decomposed for the minimum torsional distortion along the longitudinal axis. In both case studies, spot-welded joints in the structure are modeled as torsional springs. First, the rates of the torsional springs are treated as constant values obtained in the literature. Second, they are treated as design variables within realistic bounds. By allowing the change in the joint rates, it is demonstrated that the optimal decomposition can achieve the smaller distortion with less amount of joint stiffness (hence less welding spots), than the optimal decomposition with the typical joint rates available in the literature.

The work presented in this paper is still preliminary and needs extension in many directions. The immediate future work includes the extension of the framework to 3D beam-plate models, the incorporation of other design objective such as global torsion and NVH, and the adoption of more detailed joint models for, e.g., fatigue estimation. Generalizing the concept presented in this paper, it would be also possible to address the problem of simultaneously optimizing overall structural topology, decomposition, and joint properties, which is currently under investigation and to be presented at another opportunity.

References

[1] Saitou, K., and Yetis, A., 2000, "Decomposition-Based Assembly Synthesis of Structural Products: Preliminary Results," *Proceedings of the Third International Symposium on Tools and Methods of Competitive Engineering*, Delft, The Netherlands, April.

[2] Yetis, A., and Saitou, K., 2000, "Decomposition-Based Assembly Synthesis Based on Structural Considerations," *Proceedings of the 2000 ASME Design Engineering Technical Conferences*, Baltimore, Maryland, September 10–13, DETC2000/DAC-1428.

[3] Cetin, O. L., and Saitou, K., 2001, "Decomposition-Based Assembly Synthesis for Maximum Structural Strength and Modularity," *Proceedings of the 2001 ASME Design Engineering Technical Conferences*, September 9–12, 2001, Pittsburgh, PA, DETC2001/DAC-21121.

[4] Lotter, B., 1989, *Manufacturing Assembly Handbook*, Butterworths, London.

[5] Holland, J., 1975, *Adaptation in Natural and Artificial Systems*, University of Michigan Press, Ann Arbor, Michigan.

[6] Goldberg, D., 1989, *Genetic Algorithms in Search, Optimization, and Machine Learning*, Addison-Wesley, Reading, Massachusetts.

[7] Boothroyd, G., and Dewhurst, P., 1983, *Design for Assembly Handbook*, University of Massachusetts, Amherst.

[8] Boothroyd, G., Dewhurst, P., and Winston, K., 1994, *Product Design for Manufacturing and Assembly*, Marcel Dekker, New York.

[9] De Fanzio, T., and Whitney, D., 1987, "Simplified Generation of all Mechanical Assembly Sequences," IEEE Trans. Rob. Autom., pp. 640–658.

[10] Ko, H., and Lee, K., 1987, "Automatic Assembling Procedure Generation From Mating Conditions," Comput.-Aided Des., **19**, pp. 3–10.

[11] Ashley, S., 1997, "Steel Cars Face a Weighty Decision," Am. Soc. Mech. Eng., **119**(2), pp. 56–61.

[12] Chang, D., 1974, "Effects of Flexible Connections on Body Structural Response," SAE Trans., **83**, pp. 233–244.

[13] Lee, K., and Nikolaidis, E., 1998, "Effect of Member Length on the Parameter Estimates of Joints," Comput. Struct., **68**, pp. 381–391.

[14] Kim, J., Kim, H., Kim, D., and Kim, Y., 2002, "New Accurate Efficient Modeling Techniques for the Vibration Analysis of T-Joint Thin-Walled Box Structures," Int. J. Solids Struct., **39**, June, pp. 2893–2909.

[15] Garey, M. R., and Johnson, D. S., 1979, *Computers And Intractability, A Guide to the Theory of NP-Completeness*, W. H. Freeman and Company, New York.

[16] Davis, L., 1991, *Handbook of Genetic Algorithms*, Van Nostrand Reinhold, New York.

[17] Malen, D., and Kikuchi, N., 2002, Automotive Body Structure—A GM Sponsored Course in the University of Michigan, ME599 Coursepack, University of Michigan.

[18] Brown, J., Robertson, A. J., and Serpento, S. T., 2002, Motor Vehicle Structure, SAE International, Warrendale, PA.